Differences in the optical properties of vertebrate photoreceptor classes leading to axial polarization sensitivity

Nicholas W. Roberts and Helen F. Gleeson

Department of Physics and Astronomy, Schuster Laboratory, University of Manchester, Manchester M13 9PL, UK

Shelby E. Temple, Theodore J. Haimberger, and Craig W. Hawryshyn

Department of Biology, University of Victoria, P.O. Box 3020 STN CSC, Victoria, British Columbia V8W 3N5, Canada

Received July 17, 2003; revised manuscript received October 20, 2003; accepted November 14, 2003

Polarization microspectrophotometry recordings were made to investigate possible differences in the way different spectral classes of photoreceptors from coho salmon (*Oncorhynchus kisutch*) absorb linearly polarized light. The results strongly suggest that rods and cones absorb transversely illuminating polarized light differently. Cones were found to exhibit a tilted optical geometry in which the maximum absorbance occurred when the E-vector was at a small angle to the transverse axis of the outer segment. Solutions to Maxwell's equations were deduced to investigate the effect of this tilt under conditions of axial illumination. Calculations show an approximate 10% difference in the absorbance of orthogonal polarizations, suggesting the possibility of axial dichroism in the cones of this species. © 2004 Optical Society of America

OCIS codes: 330.5310, 330.5370, 260.5430, 330.4060.

1. INTRODUCTION: SENSITIVITY TO THE POLARIZED LIGHT ENVIRONMENT

The ability to detect linearly polarized light is called polarization sensitivity, and this facet of vision has been well described in a variety of vertebrates.[1–8] Much of the research has focused on polarization sensitivity in different species of teleost fishes, in particular members of the family Salmonidae.[9–13] In salmonids, there is conclusive evidence that the ultraviolet-sensitive (UVS), mid-wavelength sensitive (MWS), and long-wavelength sensitive (LWS) cones are involved in polarization sensitivity, whereas the rods and short-wavelength sensitive (SWS) photoreceptors are not. Neuronal coding of polarization information is also evident in single-unit recordings of the optic nerve and in the *torus semicircularis* of the central nervous system.[9,10] However, the biophysical mechanism by which the plane of polarization is analyzed by the cone photoreceptors is still not clearly understood, although models do exist.[13]

In order to understand the basis for how the UVS, MWS, and LWS cones relay polarization information, one needs to know specifically how polarized light interacts with individual photoreceptors. It has been assumed that in general, all teleost photoreceptors are not linearly dichroic to axial propagating polarized light[8,14,15] because of the rotational diffusion of the chromophores within the photopigment-containing membranes.[16,17] However, diffusion measurements have been reported only for non-polarization-sensitive rod photoreceptors and not for the UVS, MWS, and LWS classes of cones known to mediate polarization sensitivity in salmonids.[9,10]

In this study, we present a comparative analysis of rod and cone photoreceptors from the species coho salmon (*Oncorhynchus kisutch*) that examines transverse absorption of linearly polarized light. Polarization microspectrophotometry (PMSP) has been shown to be one of the most versatile techniques for the quantitative investigation of how single photoreceptor cells absorb polarized light.[18–23] It is well known that when a photoreceptor is illuminated from the side, owing to the stacked membrane structure of the outer segment, light polarized parallel to the transverse axis of the photoreceptor outer segment is preferentially absorbed relative to light polarized perpendicular to the transverse axis.[18,19,24–27] Consequently, comparison between the absorbance spectra for parallel and perpendicular polarized light provides information regarding the spatial orientation of the visual pigment molecules within outer-segment disk membranes. For example, ratios of absorbance perpendicular and parallel to the transverse axis of the photoreceptor (defined as the dichroic ratio by Harosi and Malerba[28]) have been measured in a variety of species.[18,19,24,27,29] In this study, we report the magnitude of absorbance with respect to the angle between the E-vector (the principal direction in which the electric field vibrates) and the transverse axis of the outer segment. Throughout this paper, this angle will be referred to as the polarization angle ϕ. We evaluate the results for significant differences between the optical properties of rods and cones through the polarization angle that yields the maximum absorbance.

2. MATERIALS AND METHODS

A. Samples and Experimental Apparatus

Spectral absorbance measurements of photoreceptors were collected from eighteen *O. kisutch* obtained from the

Robertson Creek Hatchery (Department of Fisheries and Oceans, Government of Canada). All fish were at the parr stage with a mean body mass and size (± 1 standard deviation) of 10.2 ± 3.2 g and 9.3 ± 1.7 cm, respectively. The fish were maintained on a 12:12 h light:dark photoperiod and at a temperature of 15 °C. All care and handling procedures were in accordance with the University of Victoria Animal Care Committee under the auspices of the Canadian Council on Animal Care Guidelines. Sample preparations and experimental measurements were carried out at 17 °C in a dark room with dim, deep-red illumination. All fish were first dark adapted for 1 h before being sacrificed by prolonged anesthesia with 100 mg l^{-1} Euganol (ICN Biochemicals Inc., Irvine, Calif.) until euthanized. Both eyes were then removed from the fish, each eye was hemisected, and retina was removed in Minimal Essential Media (Sigma) under infrared light. The dorsal half of the retina was teased apart onto a 35 $\times$ 50 mm, No. 1 glass microscope coverslip. Through the process of teasing apart the retinal pieces, individual photoreceptors became free from the retina, allowing the absorbance of single photoreceptors to be measured with no overlap from other spectral classes of receptors, a situation that often occurs when photoreceptors are normally mixed in the retina. A second similar microscope coverslip was placed on top of the sample, and the edges were sealed with paraffin wax.

Microspectrophotometry (MSP) and PMSP are experimental techniques regularly used for the measurement of spectral absorbance in the outer segments of vertebrate photoreceptors. Most if not all the MSP techniques currently in use are designed to make two measurements of the spectral transmittance: one through the outer segment of the photoreceptor and the other (the reference spectrum) through a clear area adjacent to the photoreceptor under investigation. The absorbance can be simply calculated as the decadic logarithm of the ratio of these two measurements. By polarizing the measurement beam for PMSP, one can obtain further information about the absorbance geometry as described in Section 1. Detailed descriptions of the MSP protocols and sample preparations used in this work have been published elsewhere,[23] and what follows gives only a brief description. Figure 1 sets out a schematic diagram of the PMSP apparatus. The measurement beam was produced by a 150-W Xenon light source (Oriel), which was coupled via a condenser assembly and optical fiber into an inverted microscope body (Zeiss). Within the condenser assembly, an infrared filter (Schott RG850, Ealing Optics) was mounted onto an electronically controlled swing arm. Placing this filter in the beam path allowed visible wavelengths to be filtered out for aligning the measurement beam onto the photoreceptor outer segment. Further, an electronic shutter was included to control the exposure time during measurements, and a feedback light-intensity controller (Oriel) was also present to maintain the intensity at the same level between the reference and sample measurements.

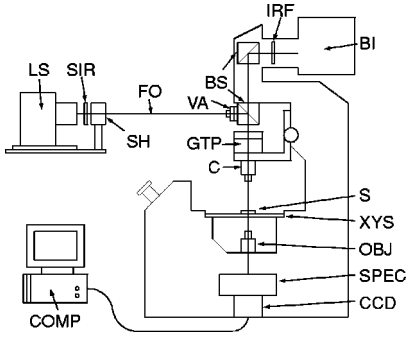

Fig. 1. Schematic diagram of the CCD microspectrophotometer. BI, back illumination; BS, beam splitter; C, 52x reflective objective as the condenser; CCD, charge-coupled device camera; COMP, custom computer software; FO, fiber optic cable; GTP, Glan-Thompson polarizer; IRF, infra-red filter; LS, Xenon lamp light source; OBJ, objective lens; S, sample; SH, shutter; SIR, infra-red filter mounted on a swing arm; SPEC, spectrograph; VA, $X-Y$ variable aperture; XYS, $X-Y$ stage.

The measurement beam passed through an $x-y$ adjustable aperture, where typically the aperture reduced the beam size to approximately 2×2 μm in the focal plane. Background illumination was produced by the 12-V, 100-W halogen lamp of the microscope. Again, an infrared filter (Schott RG850, Ealing Optics) was placed in the light path to permit viewing of the sample without bleaching. The measurement beam and the background illumination were combined by use of an Inconel coated 50% beam splitter and were imaged onto the sample via a reflecting objective (52×, 0.65 N.A., Ealing Optics) condenser. We employed a reflecting objective to compensate for chromatic aberration. The image was also viewed in real time via an infrared CCD camera (Canadian Photonics Laboratory) mounted on the microscope trinocular. A modification to the MSP protocol detailed in Ref. 23 was the inclusion of a rotatable Glan–Thompson polarizer immediately preceding the condenser assembly. The axis of the polarizer was calibrated with respect to the image orientation on the computer, allowing digital calculation ($\pm 1°$) of the required polarization measurement angle. Polarizers such as the Glan–Thompson type are limited by the small acceptance angle for which high degrees of polarization are produced. In the apparatus used, the large ratio of path length to beam size ensured that the maximum angle of incidence onto the polarizer fell within the acceptance limits. Throughout the experiment, absorbance values were measured at different polarization angles through the rotation of the polarizer. A 0.5-μm resolution, computer-controlled, motorized stage was used for positioning the sample relative to the measurement beam. The objective lens used was a glycerine immersion Zeiss Ultrafluar (100×, 1.20 N.A., infinity corrected). The objective imaged the measurement beam through a spectrograph (Acton Research), where the light was dispersed by the grating (300-nm blazing, 1200 lines/mm) allowing measurement of the 300–800-nm spectral range onto a back-illuminated cooled CCD detector (PI 1340 $\times$ 400 pixel CCD array with four-stage Peltier cooler (−50 °C) (Princeton Instruments, Roper Scientific). All measurements were made with a 0.5-s exposure time.

B. Experimental Measurement Geometry and Analysis Protocols

In this investigation, the transverse polarization absorbance of all classes of photoreceptors in *O. kisutch* were

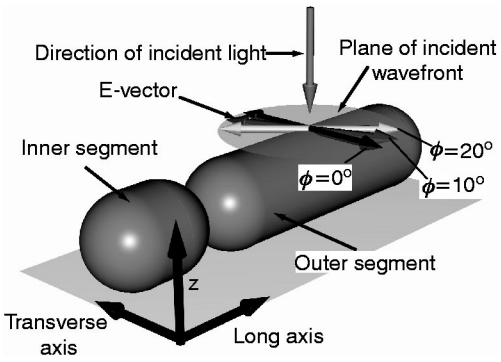

Fig. 2. Technique of polarization microspectrophotometry (PMSP). A schematic diagram of the inner and outer segments of a vertebrate ciliary photoreceptor illustrating linearly polarized light incident on the outer segment in the experimental measurement geometry. Different E-vectors are shown corresponding to the different labeled polarization angles ϕ.

measured as a function of the angle between the E-vector and the transverse axis of the photoreceptor outer segment. To reiterate, this angle will be referred to as the polarization angle ϕ. An illustration of this measurement geometry is given in Fig. 2, where different E-vectors, labeled by the polarization angle, are incident (z direction) on a photoreceptor.

The absorbance A was calculated by the formula $A = \log_{10}(I_R/I_M)$, where I_R is the intensity transmitted by the clear medium in the vicinity of the photoreceptor (reference) and I_M is the intensity transmitted by the photoreceptor.[24] In order to relate the measured absorbance spectra from different polarization angles, we had to account for any effects of inherent polarization in the measurement beam and polarization effects of the diffraction grating. This was achieved by normalizing the reference transmission spectrum to the long-wavelength limb (750–800 nm) of measured transmission spectrum for the outer segment. Once the absorbance spectra were calculated, spectra acceptance criteria were used as documented by Hawryshyn *et al.*[23] Accepted data were first smoothed by a 25-point adjacent averaging and then fitted by using a nonlinear least-squares routine (Levenberg–Marquardt algorithm), utilizing the weighted A1/A2 averaged Govardovskii template.[22] The least-squares routine allowed the calculation of the maximum absorbance value, the wavelength of maximum absorbance plus the associated errors with these measurements.[30]

For each photoreceptor examined, a series of six absorbance spectra were measured at different polarization angles, $\phi = 0°$, 20°, −20°, 10°, −10°, and 0°, by the rotation of the polarizer. An important feature is that this sequence of measurements was the same for each photoreceptor examined, because an inherent limitation in multiple measurements of spectral absorbance profiles of any photoreceptor is photobleaching.[31] The set sequence of measurements thus facilitated the comparison of first and final spectra measured at 0°. If the final value of maximum absorbance was more than two standard deviations (typically 5%) below the initial absorbance value, the photoreceptor was considered to be bleached or possibly to have moved from its original measurement position, and the data set was rejected. Here the standard deviation on the fitted maximum absorbance was calculated from the curvature matrix of the fitting routine.[30] The sequence also proved that greater values of the maximum absorbance at $\phi = \pm 10°$ or $\pm 20°$ could not be a result of bleaching. As a further control, a set of absorbance measurements were made in the stated order from both a rod and an MWS-cone photoreceptor after their respective outer segments had been bleached. The results of this test showed that the bleached baseline absorbance measurement remained constant regardless of the polarization angle.

The following results are based on the measurements from 32 rods and 48 cones ($n = 4$ UVS cones, $n = 3$ SWS cones, $n = 22$ MWS cones, and $n = 19$ LWS cones) that fitted the aforementioned criteria for acceptable absorbance spectra relative to the polarization angle and bleaching.

3. RESULTS

A. Polarization Absorbance in a Single Photoreceptor

Typical experimental absorbance spectra (solid lines) from individual photoreceptors are presented in Fig. 3, together with the fits of the Govardovskii function (dashed curves).[22] To examine the relationship between the absorbance spectra measured at different polarization

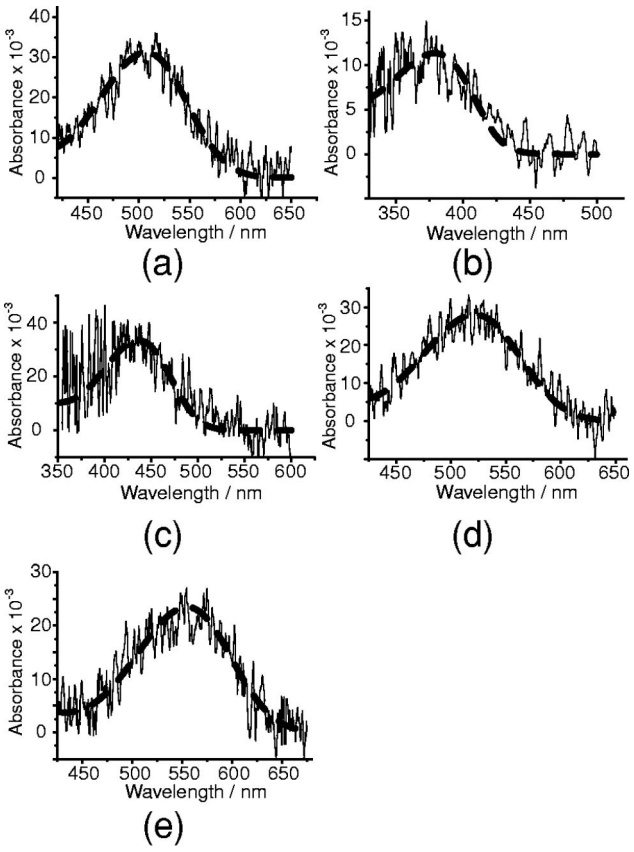

Fig. 3. Example PMSP absorbance spectra. Typical examples of experimental absorbance spectra obtained from (a) a rod, (b) a UVS cone, (c) a SWS cone, (d) a MWS cone, and (e) a LWS cone. In all panels the solid curve represents the experimental data and the dashed curve represents the fitted function of the weighted A1/A2 Govardovskii template.[22]

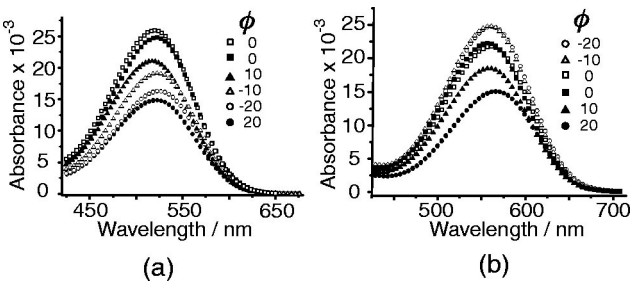

Fig. 4. Example polarization sets of fitted absorbance spectra. All curves represent the fitted functions of the weighted A1/A2 Govardovskii template for (a) a rod and (b) a LWS-cone photoreceptor. In (a) the maximum angle of absorbance $\Phi = 0°$, which corresponds to the E-vector parallel to the transverse axis of the outer segment. In (b) Φ lies at a different angle, between $-10°$ and $-20°$. In both (a) and (b) the legend indicates the polarization angle ϕ.

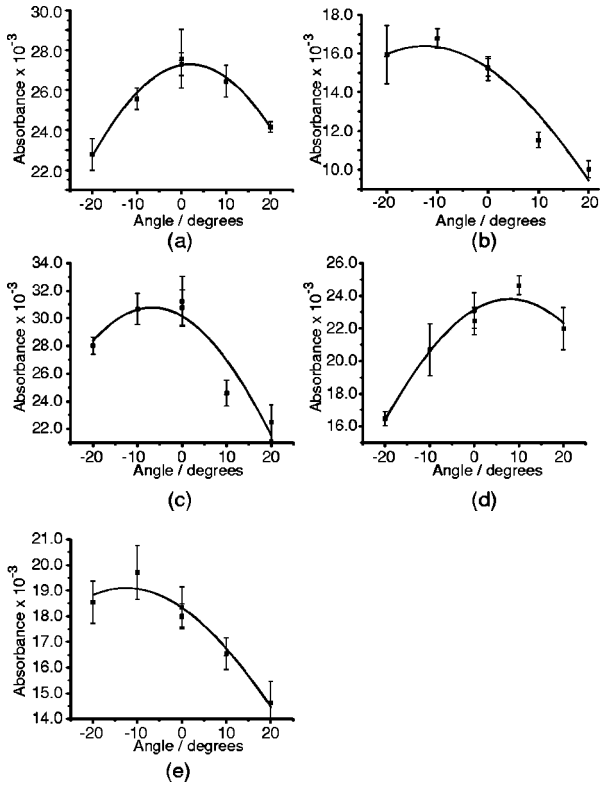

Fig. 5. Maximum absorbance values of typical individual photoreceptors as a function of polarization angle ϕ. Points correspond to experimental data and curves correspond to the fits as described by Eq. (1). (a) In the rod, the angle of maximum absorbance $\Phi = 0°$, parallel to the transverse axis of the outer segment. (b) UVS cone, (c) SWS cone, (d) MWS cone, and (e) LWS cone; the maxima of the fitted curves do not correspond to 0°, implying that Φ is not parallel to the transverse axis of the outer segment. The errors represent ± 1 standard deviation calculated from the curvature matrix.[31]

angles, the six absorbance curves calculated from the fitted Govardovskii function were plotted on a single set of axes. Figures 4(a) and 4(b) illustrate two typical examples of absorbance data sets at different polarization angles for a single rod and LWS cone, respectively. From these plots it is apparent that qualitatively, for these two photoreceptors, the polarization angle that yields the greatest value of absorbance is different. In Fig. 4(a) the polarization angle of maximum absorbance is 0° for the rod, and in Fig. 4(b) it is between $-10°$ and $-20°$ for the LWS cone.

B. Polarization Angle of Maximum Absorbance in a Single Photoreceptor

To quantitatively investigate this difference, we analyzed each photoreceptor separately with the maximum values of absorbance, calculated from each of the six fitted functions, plotted against their respective polarization angles. To measure the polarization angle of maximum absorbance Φ, we fitted the theoretical absorbance,[32]

$$a = -\log_{10}[\cos^2(\phi - \Phi)10^{-a_{\max}} + \sin^2(\phi - \Phi)10^{-a_{\min}}], \quad (1)$$

to the data again by using a nonlinear least-squares routine. In Eq. (1), a is the measured absorbance, and $a_{\max}$ and $a_{\min}$ are the maximum and the minimum absorbance, respectively. Figure 5 presents maximum absorbance value data for typical individual photoreceptors, complete with the fitted function of Eq. (1). The values of Φ deduced from the fitting of Eq. (1) in Fig. 5 are presented in Table 1, and errors are quoted as the standard deviation calculated from the curvature matrix.[30] From the values presented in Table 1, it can be seen that there is a quantitative difference in the value of Φ between the rod and cones (rod $\Phi \approx 0°$ and for the cones $\Phi \neq 0°$).

C. Differences in Φ between Rods and Cones

Figure 6 illustrates the distributions in Φ for all the measured rods and cones. A standard parametric (ANOVA) test was used to determine whether the mean value of the distribution of Φ for the rods, μ_{rod}, was significantly different from the mean value of Φ for the cones, μ_{cone}. The results of the test reveal a statistically significant difference between μ_{rod} and μ_{cone} ($F_{1,78} = 76.802$, $P < 0.001$). A Tukey high-speed-data multiple comparison was also used to investigate for significant differences in the mean values of Φ between spectral classes of photoreceptors. The results of this test are presented in Table 2 and reveal that μ_{rod} is significantly lower than $\mu_{\text{UVS cone}}$, $\mu_{\text{MWS cone}}$, and $\mu_{\text{LWS cone}}$ (in all cases $P < 0.001$). There is no significant difference among the mean values of Φ between different spectral classes of cones ($P \geq 0.601$) and between μ_{rod} and $\mu_{\text{SWS cone}}$ ($P \geq 0.289$). However, it should be noted that the sample sizes for the UVS and SWS cone measurements were $n = 4$ and $n = 3$, respectively. Consequently, the powers of the tests for the com-

Table 1. Polarization Angles of Maximum Absorbance, Φ, from Single Photoreceptors in Each Spectral Class as Illustrated in Fig. 5

Photoreceptor Type	Φ/° [a]
Rod	2 ± 1
UVS cone	12 ± 2
SWS cone	7 ± 3
MWS cone	8 ± 2
LWS cone	13 ± 3

[a] The values of Φ were obtained from the fitting routine and are ± 1 standard deviation as calculated from the matrix of curvature.[31]

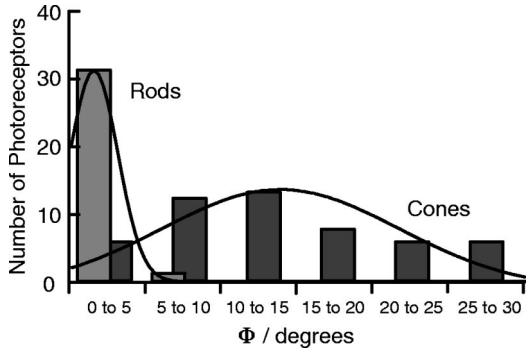

Fig. 6. Measured distribution in angle of maximum absorbance Φ of all rods and cones analyzed. The normal distribution in Φ for all photoreceptors measured illustrates a significant difference (ANOVA, $F_{1,78} = 76.802$, $P < 0.001$) between the mean values of Φ for rods and cones. The result strongly suggests that the position of maximum absorbance in cones is tilted with respect to the cones' primary axis.

Table 2. Probability Values from a Comparison (Tukey Test)[a] of Mean Values of Φ between All Spectral Classes of Photoreceptors

	UVS Cone ($n = 4$)	SWS Cone ($n = 3$)	MWS Cone ($n = 22$)	LWS Cone ($n = 19$)	Rod ($n = 32$)
UVS cone		0.601	0.990	0.982	0.000
SWS cone			0.643	0.695	0.289
MWS cone				1.000	0.000
LWS cone					0.000
Rod					

[a] The statistical test was performed with SYSTAT 9.0.

parisons between the UVS and SWS cones and other photoreceptors are <0.2. This makes it difficult to assess the real significance of these statistical data for the UVS and SWS cones, as there is a >80% chance of Type II error. However, the measurements of the UVS and SWS cones did reveal that Φ was tilted to a greater angle in these cones than for any of the more numerous rod measurements. This implies that the UVS and SWS classes have optical properties similar to those of the MWS and LWS cones measured.

4. DISCUSSION

A. Distribution in the Polarization Angle of Maximum Absorbance

The results of this study illustrate that under transverse illumination the rods and cones of *O. kisutch* absorb polarized light differently. The optical geometry appears such that the absorbance ellipsoid in the cones (and not the rods) is tilted with respect to the transverse axis of the outer segment. However, for the following two reasons it is perhaps not immediately apparent what the absolute tilt angle of the cones is.

The first reason is that the sample preparation allowed the photoreceptors to have rotational freedom about their long axes. Figure 7(a) is a schematic diagram of the outer segment of the rods (panels 1 and 2) and the cones (panels 3 and 4). For the nontilted case of the rods, the projection of the absorbance ellipsoid into the plane of the wave front shows that the angle of Φ is invariant under a 90° rotation (panels 1 and 2) of the outer segment about the long axis. This agrees with the experimental data in Fig. 6, where a narrow experimental distribution of Φ for the rods is shown. However, for the cones the projection of the absorbance varies under the 90° rotation about the long axis, from Φ = the absolute tilt angle (panel 3) to Φ = 0° (panel 4 of Fig. 7). Again, this is directly reflected in the experimental distribution of the data shown in Fig. 6, where the value of Φ for the cones varied from 2 ± 1° to 25 ± 3°. Therefore the orientational freedom of the photoreceptor greatly influences the measurement of Φ during the experiment, and the absolute value of Φ for the cones must be toward the upper limit of the measured distribution.

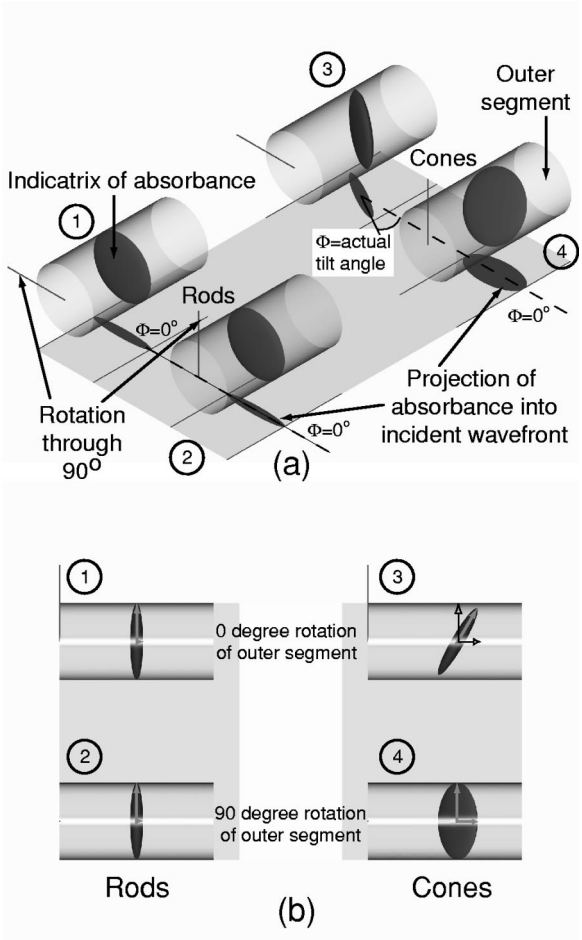

Fig. 7. Schematic diagrams of the absorbance ellipsoid in the outer segments of rods and cones. (a) Three-dimensional representation of the photoreceptor outer segments illustrating the change in the projection of the absorbance into the plane of the incident wave front and Φ as a function of the outer segment's rotational degree of freedom. For the case of the rods, panel 1 and 2 show the value of Φ to be invariant under the rotation of the outer segment. However, the value of Φ can be seen to vary from the actual tilt angle (panel 3) to Φ = 0 (panel 4) for the cones. (b) In a plan view of (a), the ratio of magnitudes of the absorbance vectors (arrows) parallel and perpendicular to the transverse axis of the outer segment corresponds to the dichroic ratio. As a direct result of the tilt, it can be seen that the dichroic ratio will be smaller in cones (panels 3 and 4) than in rods (panels 1 and 2).

The second reason concerns a possible bias in the measurement of Φ that may influence the profile of the measured distribution. When the absorbance was measured in rod photoreceptors, there was no prior selection of the cell's rotational position about the long axis for the measurement. The absorbance measurement is therefore effectively rotationally isometric for rods. However, absorbance measurements can be made in the outer segments only of double cones with the cells oriented so that the outer segments do not overlap in the field of view. If the measured tilt is consistent in direction, for example always toward the inner partitioning membrane of the outer segments, then the measured distribution of Φ will be biased toward those angles. Although this problem may seem somewhat intractable without any prior knowledge of the orientation of the tilt, in the context of this work this does not affect the conclusion that the rods and cones of *O. kisutch* absorb transversely illuminating polarized light differently.

B. Comparing the Dichroic Ratios of Rods and Cones

Consideration of both the difference in optical structure and the rotational freedom of the rods and cones also provides insight into an underlying reason why previous measurements of dichroic ratios have shown a difference between rods and cones. Several studies have consistently measured the dichroic ratios in rods to be greater than those in cones.[18,19,24,28] Figure 7(b) (panels 1–4) represents a plan view of the diagram presented in Fig. 7(a). The four illustrations again are the two limiting cases of the 0° (panels 1 and 3) and 90° (panels 2 and 4) rotation for the rods and cones about their respective long axes. In all four diagrams, the solid gray arrows represent the absorbance vectors that correspond to the principal semi-axes of the projection of the absorbance shown as the ellipsoid. However, as defined above, the dichroic ratio is a measure of the ratio of the absorbances parallel and perpendicular to the transverse axis of the outer segment. With the exception of panel 3, these two different sets of axes are coincident. Thus from the diagrams it is straightforward to see that the measured dichroic ratio will be smaller in panel 4 (cone) than in panels 1 and 2 (rod). In the case of panel 3 (cone), the absorbance parallel and perpendicular to the transverse axis of the outer segment is represented by the open black vectors. These are the resultant components of the solid gray absorbance vectors along the outer segment's principal axes. Therefore, as defined, the dichroic ratio is now the ratio of the open black vectors, illustrating that again owing to the tilt, the dichroic ratio is less in this rotational orientation of the cone than would be measured in the rods.

By this reasoning, it is possible to conclude that if the dichroic ratio is defined as the ratio between the maximum and minimum absorbance, then there may not be a difference between the dichroic ratios of rods and cones. It is perhaps worth noting that this effect may not have been seen in the past owing to certain experimental protocols. For example, in the dichroic MSP system of Harosi and MacNichol,[19] a phase difference between the carrier and the modulated (experimental) signal was always corrected for, thus intrinsically defining the maximum absorbance as parallel to the transverse axis of the outer segment.

C. Underlying Optical Structure

Consideration of the measured difference between the rods and cones poses the question of why the tilted optical structure might arise in cones and not rods. We believe there are three plausible explanations to consider in accounting for the tilted values of Φ in cones.

1. The photopigment-containing membranes are nonzero with respect to the axes of the outer segments.

In *Anchoa mitchilli* and *A. hepsetus*, it is known that the plane of the membranes within the polarization-sensitive cones is oriented parallel to the long axis of the outer segments.[7] However, this observation represents a unique example. To our knowledge, no published electron microscopy data have been presented as evidence for a consistent tilt of the membranes within the outer segments of polarization-sensitive photoreceptors in salmonids or any other polarization-sensitive vertebrate. This lack of evidence has motivated an electron microscopy investigation into the orientation of the membranes within the outer segments of salmonid photoreceptors. We hope that this study will provide a conclusive answer to the above explanation.

2. The experimental results are a measure of the tilt of the chromophore within the protein.[18,28,33]

If rotational diffusion did not occur in the cones, then the differences measured in this experiment may be explained by the value of $\Phi \neq 0°$ representing the tilt angle of the chromophore within the protein. $\Phi = 0°$ for the rods would still reflect the averaging effect of the rotational diffusion, which ensures that Φ is always perpendicular to the mean molecular orientation in the bilayer. The mean molecular orientation in a layer is commonly defined by a vector of unit length called the director.[34] However, rotational diffusion measurements have not been carried out on photoreceptors specifically involved in polarization sensitivity. Therefore we believe that this explanation is also unlikely, as rotational diffusion is considered an essential requirement for the correct function of the fluid membrane environment.

3. The mean molecular orientation of the membranes is tilted with respect to the layer normal.

This explanation relates well-known differences in the ultrastructure of rods and cones. While membranous disks containing the photopigment in rods are not connected to the outer cell membrane, the disk membranes of cones represent evaginations of a continuous cell membrane.[31] It has been shown that rod membranous disks and the outer cell membrane differ in both physical and chemical properties.[31] For example, Boesze-Battaglia and Schimmel measured significantly higher levels of cholesterol in the outer cell membrane compared with the levels in the rod disk membranes,[35] and a variety of other studies have concluded that different percentage compositions within a lipid bilayer can significantly alter the physical and orientational properties. Different director tilts within a lipid bilayer were measured as a function of different percentages of cholesterol by both Murari

et al.[36] and Macintosh.[37] Also, the tilt angle of cholesterol was shown by Brzustowicz *et al.*[38] to be a function of the bilayer composition. Therefore it is possible that different molecular compositions of the rod and cone outer segment membranes may define the different orientational and thus optical properties that have been measured in this study.

D. Optical Modeling

A clear limitation in this investigation of photoreceptor polarization sensitivity is that under natural conditions, photoreceptor illumination is axial and not transverse as in the experimental geometry used here. To investigate the effect the different optical geometries may have on the way the rods and cones absorb under axial illumination, we derived analytic solutions to Maxwell's equations for the tilted and nontilted outer segment structures. Our analysis is based on a 4×4 matrix approach, well proven and commonly used in liquid-crystal physics for modeling the optics of complex anisotropic systems.[39] Appendix A sets out the structure and derivation of the dielectric tensor used to represent the optical geometry of the outer segment under axial illumination.[40] As is detailed in Appendix A, the formulation of a complex dielectric tensor for the system accounts for all aspects of the complex refractive indices,[25,41–44] chromophore tilt,[18,28,33] rotational diffusion,[16,17] rotational degree of freedom of the photoreceptor as a whole, and the tilt of the plane of absorbance within the outer segments of the cones measured in this study. For many years, there has been much debate over the value of the refractive indices of vertebrate outer segments, and Harosi[24] and Liebman[25] have both presented detailed reviews on the subject. While the value of the linear birefringence is generally accepted as approximately 0.002, Liebman[25] points out that this value is for the whole cell and does not take into account the individual refractive indices of the membranes and surrounding isotropic cytoplasm. Thus, taking this into account, Liebmann[25] calculated the membrane birefringence to be approximately 0.02. In the calculations presented below, $n_{\parallel}$ and $n_{\perp}$ are defined as the anisotropic refractive indices parallel and perpendicular to the director of the internal membranes and $n_{external}$ as the refractive index of the cytoplasmic space. The refractive indices used were[40,41] $n_{\parallel} = 1.486$, $n_{\perp} = 1.464$, and $n_{external} = 1.365$. There is less evidence in the literature for the wavelength dependence of the complex part of the refractive index. In these calculations, the form of this complex parameter was described as a function of wavelength, in line with the results of Stavenga and Bethold[43] and Chance *et al.*[44] The chromophore tilt angle was chosen to be 16°, as detailed by several authors,[18,28,33] and the tilt angle of the absorbance ellipsoid = 15° for the case of the cone. The estimate of this angle was considered to represent a conservative value based on the experimental distribution of Φ.

Calculations of the absorbance spectra of two axial orthogonal polarized beams incident on a rod and MWS cone outer segment are presented in Figs. 8(a) and 8(b), respectively. The directions of the E-vectors are modeled such that for the two cases, they are respectively parallel and perpendicular to the plane of incidence containing the director. It can be seen that while the two polarization directions result in the same absorbance for the rod, the tilt of the plane of absorbance causes the cone to be intrinsically linearly dichroic. Figure 8(c) illustrates this effect more clearly. The absorbance of the MWS cone is plotted at λ_{max} as a function of the rotational angle of linear incident polarization. Here 0° corresponds to the E-vector parallel to the plane of incidence containing the director. The results in Fig. 8(c) show that there is approximate 10% difference between the absorbance of orthogonal axially propagating linear polarized light.

On its own, intrinsic axial dichroism of individual photoreceptors does not constitute a mechanism for polarization vision. Both Wehner[45] and Coughlin and Hawryshyn[46] set out three stages of processing considered necessary for a polarization vision system: (1) a biophysical mechanism of differential polarization absorption at the level of the photoreceptor, (2) opponent input at the internuronal level to discriminate different polarizations, and (3) a higher level of processing allowing an animal to integrate this information with other sensory inputs for complex visual tasks. The idea of intrinsic axial dichroism reported here relates to the first stage of this hierarchy. If the membrane tilt within each individual outer segment were orientated in the same direction within each outer segment, then the square cone mosaic in the salmonid retina would provide several

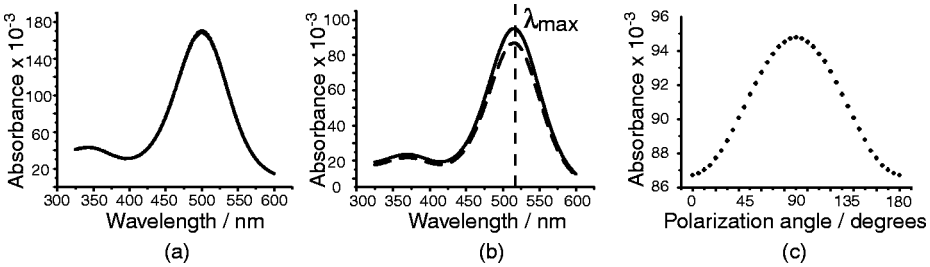

Fig. 8. Calculated absorbances from the solutions to Maxwell's equations for an axially illuminated (a) rod and (b) and (c) cone photoreceptor. (a) The absorbance spectra of the modeled rod showing the absorbance of two orthogonal polarizations corresponding to the E-vector parallel (dashed curve) and perpendicular (solid curve) to the plane of incidence which contains the director. Clearly, the two absorbance curves overlap, indicating no dichroic absorbance. (b) In the case of a MWS cone the absorbance now differs as a function of the incident polarization. Symbols are as in (a). The modulation in the absorbance at λ_{max} is shown in (c). An approximate 10% difference in the absorbance as a function of E-vector orientation shows the intrinsic axial polarization sensitivity of the cone outer segment.

overlapping spectral channels of differential polarization input, fulfilling the requirement for the unambiguous determination of E-vector orientation. Further work is currently underway with the aim of investigating this mechanism by measuring axial absorbance of individual photoreceptors under full control of the measurement geometry with an optical trapping system. Further work is also focusing on understanding the various aspects in the neural processing of both spectral and polarization information in salmonids at the level of the horizontal and bipolar cells in the outer plexiform layer. This level of processing is the link between the stages 1 and 2 of a polarization vision system outlined above. It could also be suggested that the biophysical mechanism of differential absorption proposed here could be applicable to a wide range of vertebrates, providing a similar unifying mechanism of polarization sensitivity as exists for invertebrates. However, it should also be noted that the required square cone mosaics in the retina, while common in many species of teleost, are not a typical feature in reptilian or avian retinas, groups known to contain polarization-sensitive members.

E. Context of These Results with Respect to Previous Electrophysiological Recordings

Although all double cones were free to rotate about their respective long axes within the sample preparation, the structure of the cell dictates that absorbance measurements can be made only when the outer segment under investigation is not overlapping or being overlapped by the neighboring outer segment. Each outer segment is also not allowed to rotate independently with respect to its neighbor. The Tukey test (Table 2) illustrated that there was no significant difference ($P = 1.00$) between the values of Φ for the MWS and LWS outer segments. In a square ordered mosaic, these results would imply that the MWS and LWS outer segments of a single double cone would exhibit the same sensitivity to polarized light. With similar neural wiring of both spectral channels, this may be in agreement with previous studies of the MWS and LWS OFF responses from multiunit recordings in the optic nerve.[46] In this work it was found that the MWS and LWS spectral channels share the same function of polarization sensitivity, both exhibiting a maximum response to horizontally polarized light.

It is also known from several electrophysiological studies that while the UVS, MWS, and LWS channels exhibit polarization sensitivity, the SWS channel does not.[9,10] Solely on the basis of the measurements and the calculations in the current study, the measured tilt in SWS cones does imply that the SWS class could also exhibit a differential response to axial illuminating polarized light. However, this fact is not necessarily in contradiction with the electrophysiological recordings. Although the measurements in single units of the optic nerve reveal that the SWS cones do not mediate polarization sensitivity, these measurements are made at a considerably later stage of neural processing than the MSP measurements. It is possible that any differential response of the cones is negated in some way by the neural processing.

5. CONCLUSIONS

To our knowledge, this is the first report of significant differences between the way rod and cone photoreceptors absorb linearly polarized light. The results strongly suggest that the position of maximum absorbance in cones is tilted with respect to the primary axes of the cell. A plausible hypothesis was presented for the basis of this tilt, based on structural and compositional differences resulting in the different optical properties. Finally, analytic solutions to Maxwell's equations were deduced to investigate the effect of the tilt on the absorbance under axial illumination of the outer segment. The results of this part of the study suggest the possibility of axial dichroism within the cone photoreceptors that specifically mediate polarization vision in salmonid fishes. However, further experimental work is required both to directly measure differential axial polarization absorbance and to study the implications of the interaction with other possible mechanisms of polarization sensitivity.[13] In general, it is possible that with the correct orientation of this tilt and spatial arrangement of the photoreceptors in the retina, axial dichroism of vertebrate photoreceptors may provide a similar unifying mechanism of polarization sensitivity that exists among many species of invertebrate.

APPENDIX A: VERTEBRATE PHOTORECEPTOR DIELECTRIC TENSORS AND SOLUTIONS TO MAXWELL'S EQUATIONS

For calculation of the absorbance of an anisotropic layered structure, the complex dielectric tensor must first be derived for the system. The derivation that follows examines the dielectric tensor of the vertebrate outer segment under axial illumination. A similar derivation can be made for a photoreceptor under transverse illumination, with the corresponding change in the coordinate system and the dielectric tensor. The full description of the electromagnetic theory presented here will be the subject of a forthcoming paper.[40] The following angles used to describe the coordinate transformations are detailed in Fig. 9.

Assuming that the absorption along the long axis of the chromophore is very much greater than along the other two orthogonal axes,[47] the absorption tensor of the chromophore is given by

$$\epsilon_{\text{axial}} = \begin{bmatrix} \alpha & 0 & 0 \\ 0 & 0 & 0 \\ 0 & 0 & 0 \end{bmatrix}, \tag{A1}$$

where α represents the imaginary part of the dielectric constant. The chromophore resides at an angle θ to the principal axis of the opsin protein, where θ is known to be approximately 16° in vertebrate photoreceptors.[18,28,33] Therefore rotating the chromophore frame of reference into that of the protein gives

$$\epsilon_{\text{axial}}(\theta) = R_{\text{axial}}(\theta)\epsilon_{\text{axial}}R^{-1}_{\text{axial}}, \tag{A2}$$

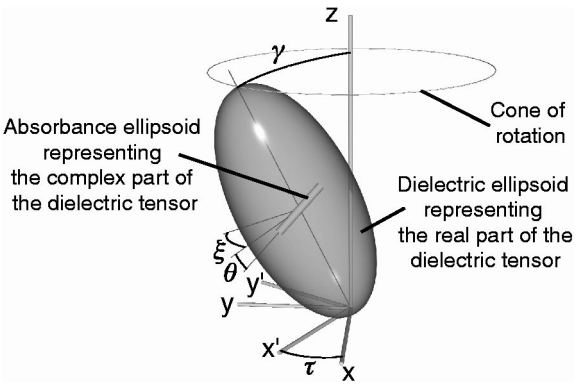

Fig. 9. Coordinate system used in the construct of the dielectric tensor. Principal axes of the dielectric ellipsoid represent the semi-axes of the uniaxial optical structure. Labeled angles show the parameters used for the transformation from the molecular to the laboratory frame of reference.

where

$$R_{\text{axial}}(\theta) = \begin{bmatrix} \cos\theta & 0 & -\sin\theta \\ 0 & 1 & 0 \\ \sin\theta & 0 & \cos\theta \end{bmatrix}. \tag{A3}$$

Multiplying out Eq. (A2) and including the real dielectric constants of the protein frame of reference produces the result that the full dielectric tensor becomes

$$\epsilon_{\text{axial}}(\theta) = \begin{bmatrix} \epsilon_1 + \alpha\cos^2\theta & 0 & \alpha\sin\theta\cos\theta \\ 0 & \epsilon_2 & 0 \\ \alpha\sin\theta\cos\theta & 0 & \epsilon_3 + \alpha\sin^2\theta \end{bmatrix}, \tag{A4}$$

where ϵ_i and $i = 1, 2, 3$, represent the three real dielectric constants and in a uniaxial system, as is being considered here, $\epsilon_1 = \epsilon_2$. Several rotational degrees of freedom can now also be accounted for with similar rotational transformations. With reference to the angles defined in Fig. 9, the rotational diffusion of the system ξ, the bilayer tilt γ, and the rotational degree of freedom for the whole outer segment around the system's long axis τ (in Fig. 9 this is the rotation from the x', y', z axis system to the x, y, z system) can be included in the dielectric tensor by transformations similar to those in Eq. (A3) to give

$$\epsilon_{\text{axial}}(\tau,\ \gamma,\ \xi,\ \theta) = \begin{bmatrix} AA & BB & DD \\ BB & CC & EE \\ DD & EE & FF \end{bmatrix}, \tag{A5}$$

where the substitutions used are

$$\begin{aligned}
a &= (\epsilon_1 + \alpha\cos^2\theta)\cos^2\xi + \epsilon_2\sin^2\xi, \\
b &= (\epsilon_1 - \epsilon_2 + \alpha\cos^2\theta)\cos\xi\sin\xi, \\
c &= (\epsilon_1 + \alpha\cos^2\theta)\sin^2\xi + \epsilon_2\cos^2\xi, \\
d &= \alpha\sin\theta\cos\theta\cos\xi, \\
e &= \alpha\sin\theta\cos\theta\sin\xi, \\
f &= \epsilon_3 + \alpha\sin^2\theta, \\
A &= a\cos^2\gamma - 2d\cos\gamma\sin\gamma + f\sin^2\gamma, \\
B &= b\cos\gamma - e\sin\gamma, \\
C &= c, \\
D &= d\cos^2\gamma - d\sin^2\gamma + (a - f)\cos\gamma\sin\gamma, \\
E &= b\sin\gamma + e\cos\gamma, \\
F &= a\sin^2\gamma + 2d\cos\gamma\sin\gamma + f\cos^2\gamma, \\
AA &= A\cos^2\tau - 2B\cos\tau\sin\tau + C\sin^2\tau, \\
BB &= B\cos^2\tau - B\sin^2\tau + (A - C)\cos\tau\sin\tau, \\
CC &= A\sin^2\tau + 2B\cos\tau\sin\tau + C\cos^2\tau, \\
DD &= D\cos\tau - E\cos\tau, \\
EE &= D\sin\tau + E\cos\tau, \\
FF &= F.
\end{aligned} \tag{A6}$$

From the construction of the complex dielectric tensor, Maxwell's equations can be solved by using a standard 4 × 4 matrix approach. The individual steps of this technique can be found in several texts (for example, for a derivation in S.I. units see Ref. 48) and therefore will not be set out in full in this appendix. An analytic solution for the optical tensor of a single-layer system under axial illumination can be found as

$$\Delta = \begin{bmatrix} 0 & 1 & 0 & 0 \\ AA - \dfrac{DD^2}{FF} & 0 & BB - \dfrac{DD \times EE}{FF} & 0 \\ 0 & 0 & 0 & 1 \\ BB - \dfrac{DD \times EE}{FF} & 0 & CC - \dfrac{EE^2}{FF} & 0 \end{bmatrix}. \tag{A7}$$

For correct modeling of the outer segment of the photoreceptor, the multiple layer structure must be accounted for. The way this is incorporated into the model differs depending on whether the photoreceptor is illuminated transversely or axially. Under axial illumination, a layered structure can easily be modeled through a successive multiplication of the optical tensor with an isotropic dielectric tensor defining each surrounding intracellular space to calculate the overall optic tensor. This also allows for the rotational diffusion to be included in the model, the value of ξ being set simply with a random-number generator (between the limits of 0 and 360°) from one anisotropic layer to the next. By consideration of the boundary conditions, three generalized field vectors of the external incident, transmitted, and reflected waves can be related to the internal electric-field components. This allows the calculation of the 2 × 2 complex amplitude transmission and reflection matrices, the determination of which completes the problem.

ACKNOWLEDGMENTS

The authors thank Robertson Creek Hatchery (Department of Fisheries and Oceans, Canada) for supplying the experimental animals and J. Lydon for very helpful dis-

cussions at the outset of this study. This research was supported by a travel fellowship to N. W. Roberts from the Journal of Experimental Biology, operating and equipment grants to H. F. Gleeson from the Engineering and Physical Sciences Research Council of Canada, and to C. W. Hawryshyn from the Natural Sciences and Engineering Research Council of Canada.

Correspondence should be addressed to C. W. Hawryshyn (e-mail, chawrysh@uvic.ca) and H. F. Gleeson (e-mail, helen.gleeson@man.ac.uk).

REFERENCES

1. M. J. Freake, "Evidence for orientation using the e-vector direction of polarised light in the sleepy lizard *Tiliqua rugosa*," J. Exp. Biol. **202**, 1159–1166 (1999).
2. K. Adler and J. B. Phillips, "Orientation in a desert lizard (*Uma notata*): time-compensated compass movement and polarotaxis," J. Comp. Physiol. A **156**, 547–552 (1985).
3. D. H. Taylor and K. Alder, "Spatial orientation by salamanders using plane polarised light," Science **181**, 285–287 (1973).
4. K. P. Able, "Skylight polarization patterns at dusk influence migratory orientations in birds," Nature **299**, 550–551 (1982).
5. J. B. Phillips and F. R. Moore, "Calibration of the sun compass by sunset polarized patterns in a migratory bird," Behav. Ecol. Sociobiol. **31**, 189–193 (1992).
6. C. W. Hawryshyn and W. N. McFarland, "Cone photoreceptor mechanisms and the detection of polarized light in fish," J. Comp. Physiol. **160**, 459–465 (1987).
7. B. A. Fineran and J. A. C. Nicol, "Studies on the photoreceptors of *Anchoa mitichilli* and *A. hepsetus* (Engranlidae) with particular reference to the cones," Philos. Trans. R. Soc. London Ser. B **283**, 25–60 (1978).
8. T. H. Waterman, "Natural polarised light and e-vector discrimination by vertebrates," in *Light as an Ecological Factor II* (Blackwell, Oxford, UK, 1975), pp. 305–335.
9. D. C. Parkyn and C. W. Hawryshyn, "Spectral and ultraviolet-polarization sensitivity in juvenile salmonids: a comparative analysis using electrophysiology," J. Exp. Biol. **203**, 1173–1191 (2000).
10. D. J. Coughlin and C. W. Hawryshyn, "A cellular basis for polarized-light vision in rainbow trout," J. Comp. Physiol. A **176**, 261–272 (1995).
11. C. W. Hawryshyn, M. G. Arnold, E. Bowering, and R. L. Cole, "Spatial orientation of rainbow trout to plane-polarised light: the ontogeny of e-vector discrimination and spectral sensitivity characteristics," J. Comp. Physiol. A **166**, 566–574 (1990).
12. I. N. Flamarique and H. I. Browman, "Foraging and prey-search behaviour of small juvenile rainbow trout (*Oncorhynchus mykiss*) under polarized light," J. Exp. Biol. **204**, 2415–2422 (2001).
13. I. N. Flamarique, C. W. Hawryshyn, and F. I. Harosi, "Double cone internal reflection as a basis for polarization detection in fish," J. Opt. Soc. Am. A **15**, 349–358 (1998).
14. A. W. Snyder, "Physics of vision in compound eyes," in *Handbook of Sensory Physiology VII/6A*, H. Autrum, ed. (Springer-Verlag, Berlin, 1979), pp. 284–285.
15. M. F. Land and D. E. Nilsson, "Light and Vision," in *Animal Eyes* (Oxford U. Press, Oxford, UK, 2002), pp. 29–31.
16. P. K. Brown, "Rhodopsin rotates in the visual receptor membrane," Nature New Biol. **236**, 35–38 (1972).
17. R. A. Cone, "Rotational diffusion of rhodopsin on the visual receptor membrane," Nature New Biol. **236**, 39–43 (1972).
18. P. A. Liebman, "In situ microspectrophotometric studies on the pigments of single retinal rods," Biophys. J. **2**, 161–178 (1962).
19. F. I. Harosi and E. F. MacNichol, Jr., "Dichroic microspectrophotometer: a computer assisted, rapid, wavelength scanning photometer for measuring the linear dichroism of single cells," J. Opt. Soc. Am. **64**, 903–918 (1974).
20. E. R. Loew and H. J. A. Dartnall, "Vitamin A_1/A_2-based visual pigment mixtures in cones of the rudd," Vision Res. **16**, 891–896 (1976).
21. J. M. Bowmaker, "Microspectrophotometry of vertebrate photoreceptors," Vision Res. **24**, 1641–1650 (1984).
22. V. I. Govardovskii, F. Fyhrquist, T. Reuter, D. G. Kuzmin, and K. Donner, "In search of the visual pigment template," Visual Neurosci. **17**, 509–528 (2000).
23. C. W. Hawryshyn, T. J. Haimberger, and M. E. Deutschlander, "Microspectrophotometric measurements of vertebrate photoreceptors using CCD-based detection technology," J. Exp. Biol. **204**, 2431–2438 (2001).
24. F. I. Harosi, "Microspectrophotometry and optical phenomena: birefringence, dichroism, and anomalous dispersion," in *Vertebrate photoreceptor optics*, J. M. Enoch and F. L. Tobey, Jr., eds. (Springer-Verlag, Berlin, 1981), pp. 337–397.
25. P. A. Liebman, "Birefringence, dichroism and rod outer segment structure," in *Photoreceptor Optics*, A. W. Snyder and R. Menzel, eds. (Springer-Verlag, Berlin, 1975), pp. 119–214.
26. A. G. Palacios, R. Strivastava, and T. H. Goldsmith, "Spectral and polarization sensitivity of photocurrents of amphibian rods in the visible and ultraviolet," Visual Neurosci. **15**, 319–331 (1998).
27. R. A. Weale, "On the linear dichroism of frog rods," Vision Res. **11**, 1373–1385 (1971).
28. F. I. Harosi and F. E. Malerba, "Plane polarized light in microspectrophotometry," Vision Res. **15**, 379–388 (1975).
29. F. I. Harosi, "Linear dichroism of rods and cones," in *NATO Advanced Study Institute Series, Series A: Life Sciences* (Plenum, New York, 1975), pp. 55–65.
30. P. R. Bevington, *Data Reduction and Error Analysis for the Physical Sciences* (McGraw Hill, New York, 1994), pp. 242–246.
31. A. I. Cohen, "Rods and cones," in *Handbook of Sensory Physiology VII/2*, M. G. F. Fuortes, ed. (Springer-Verlag, Berlin, 1972), pp. 63–110.
32. M. Born and E. Wolf, *Principles of Optics*, 7th expanded ed. (Cambridge U. Press, Cambridge, UK, 1999), pp. 218–219.
33. G. Gröbner, C. G. Burnett, A. Choi, J. Mason, and A. Watts, "Observations of light-induced structural changes of retinal within rhodopsin," Nature **405**, 810–813 (2000).
34. P. Collings and M. Hird, *Introduction to Liquid Crystals* (Taylor & Frances, London, 1997), pp. 1–5.
35. K. Boesze-Battaglia and R. J. Schimmel, "Cell membrane lipid composition and distribution: Implications for cell function and lessons learned from photoreceptors and platelets," J. Exp. Biol. **200**, 2927–2936 (1997).
36. R. Murari, M. P. Murari, and W. J. Baumann, "Sterol orientations in phosphatidycholine liposomes as determined by deuterium NMR," Biochemistry **25**, 1062–1067 (1986).
37. T. J. McIntosh, "The effect of cholesterol on the structure of phosphatidycholine bilayers," Biochim. Biophys. Acta **513**, 43–58 (1973).
38. M. R. Brzustowicz, W. Stillwell, and S. R. Wassall, "Molecular organization in polyunsaturated phospholipid membranes: a solid state ^{2}H NMR investigation," FEBS Lett. **451**, 197–202 (1999).
39. D. Berreman, "Optics in stratified and anisotropic media: 4×4-matrix formulation," J. Opt. Soc. Am. **62**, 502–510 (1972).
40. N. W. Roberts and H. F. Gleeson, Department of Physics, University of Manchester, Manchester, M13 9PL, UK, are preparing a manuscript to be called "The absorbance of polarized light by vertebrate photoreceptors."
41. P. A. Liebman, W. S. Jagger, M. W. Kaplan, and F. G. Bargoot, "Membrane structure changes in rod outer segments associated with rhodopsin bleaching," Nature **251**, 31–36 (1974).

42. J. N. Israelchvili, R. A. Sammut, and A. W. Snyder, "Birefringence and dichroism of photoreceptors," Vision Res. **16**, 47–52 (1976).
43. D. G. Stavenga and H. H. van Barneveld, "On dispersion in visual photoreceptors," Vision Res. **15**, 1091–1095 (1974).
44. B. Chance, R. Perry, L. Akerman, and B. Thorell, "Highly sensitive recording microspectrophotometer," Rev. Sci. Instrum. **30**, 735–741 (1959).
45. R. Wehner, "The hymenopteran skylight compass: matched filtering and parallel coding," J. Exp. Biol. **146**, 63–85 (1989).
46. D. J. Coughlin and C. W. Hawryshyn, "A cellular basis for polarized-light vision in rainbow trout," J. Comp. Physiol. A **176**, 261–272 (1995).
47. R. Mathies and L. Stryer, "Retinal has a dipolar vertically excited singlet state: implications for vision," Proc. Natl. Acad. Sci. U.S.A. **73**, 2169–2173 (1976).
48. R. M. A. Azzam and N. M. Bashara, *Ellipsometry and Polarised Light* (Elsevier, Amsterdam, 1987), pp. 340–352.